Available online at www.sciencedirect.com

SciVerse ScienceDirect

Ceramics International 38 (2012) 6665–6670

CERAMICS INTERNATIONAL

www.elsevier.com/locate/ceramint

Surface characterization of Au–ZnO nanowire films

Farid Jamali-Sheini[a,*], Ramin Yousefi[b], K.R. Patil[c]

[a]Department of Physics, Ahwaz Branch, Islamic Azad University, Ahwaz, Iran
[b]Department of Physics, Masjed-Soleiman Branch, Islamic Azad University, Masjed-Soleiman, Iran
[c]Physical and Materials Chemistry Division, National Chemical Laboratory, Pune 411008, India

Received 1 April 2012; received in revised form 16 May 2012; accepted 17 May 2012
Available online 26 May 2012

Abstract

Au–ZnO nanowire films have been synthesized by annealing Zn foils coated with a thin layer of gold. An X-ray diffraction study found that the synthesized ZnO consists mainly of a hexagonal wurtzite structure along with a small amount of $AuZn_3$ phase. Scanning electron images showed that the ZnO wires extend to several microns in length. X-ray photoelectron spectroscopy studies confirmed the oxidation states of Au and Zn. An asymmetric O 1s peak indicates the presence of oxygen in an oxide layer and O–H groups on the films surfaces. Photoluminescence (PL) spectra showed different visible peaks for pre-annealed films, while for annealed films an UV peak appeared. In addition, the PL analysis showed that the overall intensity of photoluminescence decreased significantly after the films were annealed. Raman spectroscopy results also indicated that the crystalline quality of the films improved with annealing. This could be attributed to a decrease in oxygen vacancies and/or absorption of O–H groups on the surface of ZnO film. The highly hydrophilic surface with a water contact angle of $\sim 155^{\circ}$ was obtained after annealing in air.

Keywords: Au–ZnO; Highly hydrophilic; Nanowires; XPS

1. Introduction

One dimensional (1D) ZnO nanostructures have attracted much interest at research and industrial levels due to their unique optical, electrical, magnetic, acoustic and chemical properties. These structures were found to be promising candidates in many technological applications such as piezoelectrics, optoelectronics, chemical sensors, etc. [1].

The most energetically favorable structure of ZnO is wurtzite with a direct bandgap of 3.37 eV at room temperature. It is known to possess n-type conduction owing to its native donor defects such as oxygen vacancies [2]. Many low dimensional ZnO structures such as particles, wires, tubes, belts and rings have been reported with unique properties over the past decade. For example, the mobility of charge carriers in nanowires is reported to be 100 times higher than it is in spherical particles [3]. Various techniques, including thermal oxidation and/or evaporation [4–7], pulsed laser deposition [8], chemical vapor deposition [9,10], plasma-assisted molecular beam epitaxy [11], solvothermal [12] and sonochemical methods [13] and electrochemical deposition [14,15] have been used to deposit nanostructured ZnO materials.

To modify electrical, optical and other properties of ZnO nanostructures/films, it is practical to dope/decorate ZnO with other elements. The efficiency of the dopant element depends mainly on its electronegativity and ionic radius affecting the surrounding local lattice environment. Cationic doping of ZnO has been achieved by replacing Zn^{2+} ions with ions of elements having different valences such as Li^{1+}, Mn^{2+} and Sn^{4+} [1]. Despite many reports describing doping procedures, the doping effects of noble metals on structural and physical properties of ZnO nanostructures have not yet been investigated in detail and is still of considerable interest. Several researchers have recently attempted to enhance the sensing properties of metal oxides by doping with noble metal-based catalysts such as Au, Pd and Pt [16–19]. It is believed that doping/decorating ZnO with a noble metal may lead to novel or

*Corresponding author. Tel.: +98 611 3348420 24; fax: +98 611 3329200.
E-mail addresses: faridjamali2003@yahoo.com, faridjamali@iauahvaz.ac.ir (F. Jamali-Sheini).

0272-8842/$36.00
http://dx.doi.org/10.1016/j.ceramint.2012.05.054

enhanced performance. Moreover, little work has so far been performed on surface properties of nanostructures modified by these metals.

In addition to the optical and electrical properties that have been altered by dopants, surface wettability could be also impacted by doping materials. Recently, there has been increasing interest in controlling this property. It is usually quantified by measuring the angle of water contact and depends on the surface free energy and the geometric structure of the surface [20,21]. In addition, for technological application, it is important to be able to manipulate wettability of different surfaces. To this end, wettability of synthesized (Au–ZnO nanowire) films has been investigated. It has been found that the Au–ZnO nanowire film surface is highly hydrophilic. So films have been synthesized by annealing (thermal oxidation/diffusion) zinc foils coated with a thin layer of gold in air. Despite being simple, inexpensive, of large scale and of low temperature ($T \leq 400$ °C), this method is limited by solubility, i.e. the yield of dopant concentration is not high enough. X-ray diffraction, X-ray photoemission spectroscopy, photoluminescence, Raman and contact angle analyses have been carried out to study the properties of ZnO nanostructures.

2. Experimental details

ZnO nanowires were grown by the following procedure: (i) Zn foils (99.99%, Alfa Aesar), used as substrates and source materials, were ultrasonically cleaned in acetone and methanol for 10 min in each solvent; (ii) a thin layer of gold (thickness ~60 nm) was deposited on the substrates by vacuum evaporation at base pressure of 1×10^{-5} mbar; the gold layer thickness was measured using the Taly step method (Taylor–Hobson); this thin film serves as a catalyst for the growth of ZnO nanostructures; (iii) after gold deposition, the substrates were annealed at 400 °C in a furnace in air at atmospheric pressure for 4 h.

The synthesized ZnO nanostructures were characterized by an X-ray diffractometer (XRD; Model-D8, Advance, Bruker AXS) with Cu Kα radiation ($\lambda = 1.5406$ Å), and a scanning electron microscope (SEM; JEOL, JSM-6360A) at 20 kV operating voltage and 60 μA emission current. The elemental composition was obtained by an energy-dispersive X-ray spectrometer (EDS) attached to the SEM instrument operating at 20 kV. Collection time was 80 s and the number of spots analyzed was 4 each of 25 μm^2 area. The composition of the film was analyzed by X-ray photoelectron spectroscopy (XPS, VG Microtech ESCA 3000) measurement. XPS spectra were recorded at 10^{-10} mbar base pressure using Mg Kα radiation (1253.6 eV, line width 0.7 eV) generated at 150 W. The optical properties were obtained from photoluminescence (PL) spectra recorded at room temperature using a Xenon lamp as a source (PL Spectrometer, Perkin Elmer-LS-55). The exciting wavelength was chosen to be 325 nm. Raman spectra were measured using a Raman spectrometer (Thermo Nicolet Almega), with Nd:YLF laser (wavelength 532 nm, 30 mW) as an excitation source over the wavelength range 200–650 nm. The measurement of water contact angle (WCA) was performed by a homemade measurement system at ambient temperature. Small water droplets (5 μL) were dropped on the surface of the specimen and the WCA was recorded by a digital camera. The WCAs were obtained at 4 different points on each specimen by measuring the angle between the surface of the specimen and water droplet boundary on the surface.

3. Results and discussion

The XRD patterns of the Zn foils, with and without pre-coating a thin layer of gold annealed at 400 °C, are shown in Fig. 1. Both XRD patterns exhibit a set of well defined diffraction peaks, indicating formation of polycrystalline phases. The peaks are indexed to the hexagonal wurtzite ZnO structure. In the annealed Zn foil pre-coated with gold layer, peaks corresponding to metallic Au and Au–Zn alloy are also observed.

Fig. 2(a) and (b) shows typical SEM images of the Zn foil pre-coated with a thin layer of gold annealed at 400 °C for 4 h in air. Fig. 2(a) clearly shows formation of ZnO nanowires on the entire substrate surface. A highly magnified image exhibits tapering in the nanowire and is shown in Fig. 2(b). The average diameters and lengths of these wires are in the range of a few nanometers and several microns, respectively. In the annealed Zn foil which was not pre-coated with a thin layer of gold, no nanowires were observed on the Zn foil. EDS was performed to investigate the chemical composition of the annealed Zn foil pre-coated with a thin layer of gold (Au–ZnO nanowires film) and the result is shown in Fig. 3. The presence of Zn, O and Au was observed. No peaks corresponding to other materials were detected.

The chemical bindings of Au, Zn and O, present on the surface of Au–ZnO nanowire films have been characterized

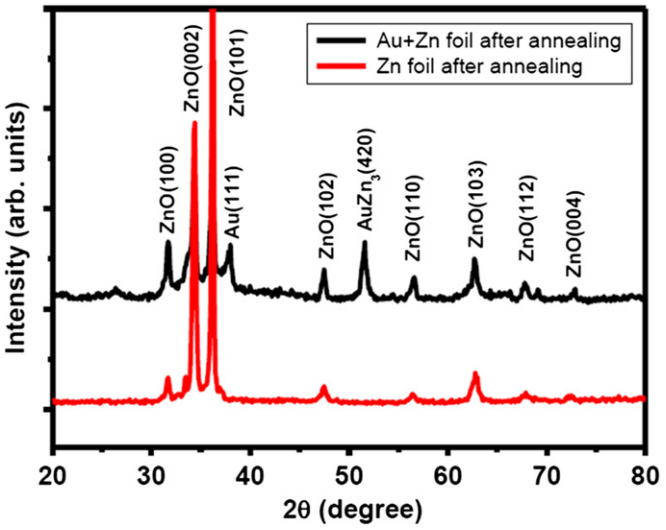

Fig. 1. XRD patterns of the Zn foil with and without pre-coating a thin layer of gold annealed at 400 °C for 4 h.

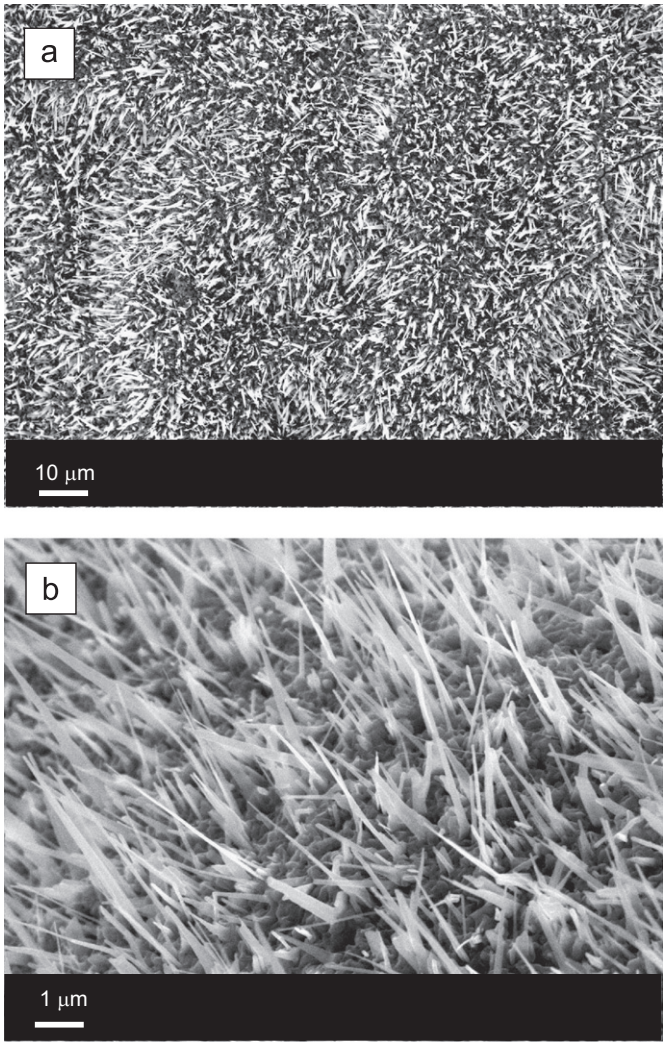

Fig. 2. SEM images of the Zn foil pre-coated with a thin layer of gold annealed at 400 °C for 4 h at low (a) and high (b) magnifications.

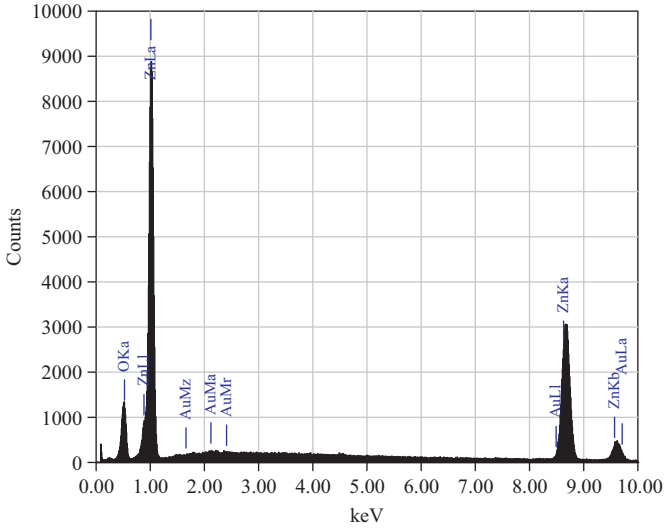

Fig. 3. EDS of the Zn foil pre-coated with a thin layer of gold annealed at 400 °C for 4 h (Au–ZnO nanowires film).

by the XPS technique. Binding energy is calibrated by taking the C 1s peak (285 eV) as a reference. Typical high resolution scans of Au 4f–Zn 3p, Zn 2p and O 1s are

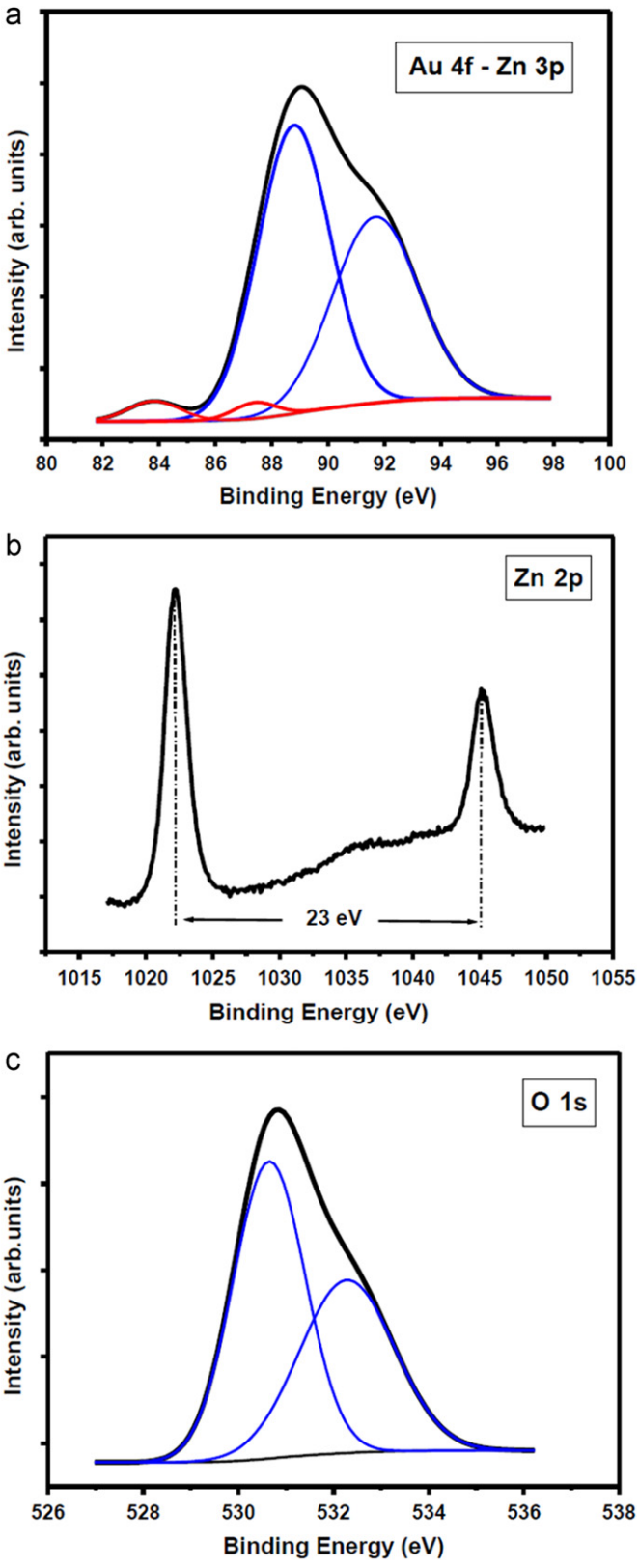

Fig. 4. XPS spectra of the Au–ZnO nanowire film: (a) Au 4f–Zn 3p region, (b) Zn 2p region, and (c) O 1s region.

shown in Fig. 4(a), (b) and (c), respectively. The Au 4f–Zn 3p peak (Fig. 4(a)) has a shoulder on the low binding energy side, which could be deconvoluted by means of a standard software using a Shirly type background correction and symmetric Gaussian curves. Four separate peaks were resolved, namely Au 4f $_{7/2}$ (83.4 eV), Au 4f $_{5/2}$ (87.4 eV) for gold and Zn 3p $_{3/2}$ (88.7 eV) and Zn 3p $_{1/2}$ (91.6 eV) for zinc. The binding energy of the Zn 2p $_{3/2}$ and Zn 2p $_{1/2}$ peaks are centered at 1022.2 eV and 1045.2 eV, respectively as shown in Fig. 4(b). The spin orbit splitting of 23 eV indicates that the ion valence state is Zn^{2+} [22]. The scan of the O 1s spectrum is shown in Fig. 4(c). The asymmetric peak was deconvoluted into two components with binding energies of 530.6 eV and 532.2 eV, attributed to O–Zn and O–H bond formation, respectively. The O–H bonds can be attributed to formation of loosely bound oxygen at the surface (absorbed oxygen and O–H groups) or to O^{2-} ions in the oxygen-deficient regions [23]. Formation of O–Zn is attributed to O^{2-} ions in the ZnO lattice. The area ratio of these two Gaussians is 43:57, which indicates that only 57% of the oxygen ions are located at the fully oxidized ZnO lattice. They are associated with lattice defects in the films, such as oxygen vacancy, interstitial zinc, zinc vacancy and interstitial oxygen, which are consistent with the background in the photoluminescence spectra in the following section.

As the PL properties of ZnO are sensitive to oxygen vacancy, the room temperature PL spectra of specimens were studied. The results of PL measurements related to the pre- and post-annealed Zn and Au pre-coated Zn foils are shown in Fig. 5. It can be observed that for Au pre-coated Zn foils there is no peak in the UV region, while a UV peak at 386 nm appears for annealed films. The presence of the UV peak after annealing indicates that the crystallinity of the film has been improved. By careful observation in the visible region, it can be seen that the visible peak positions (450–650 nm) in all spectra are the same with different intensities. After annealing, the intensities of visible peaks were observed to decrease significantly compared to those obtained before annealing. The decrease in visible peaks intensities indicates that the number of defects, which trap photo-generated free electrons and holes in the film, has decreased [24]. Oxygen vacancies were believed to be the main defects causing the visible PL in ZnO [25,26]. The decrease in intensities is due to the diffusion of oxygen gas and/or impurities ions into the oxygen vacancies of ZnO during the annealing process [27,28].

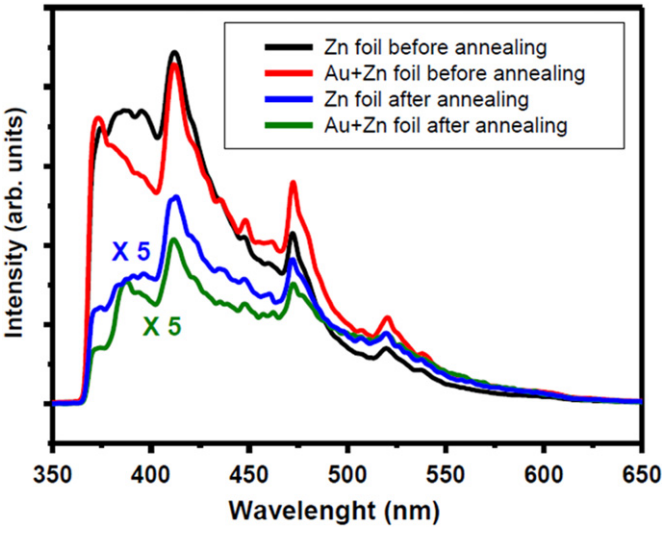

Fig. 5. PL spectra of the pre- and post-annealed Zn and Au pre-coated Zn foils.

Raman measurements give information about material quality, phase and purity in order to understand transport properties and phonon interaction with the free carriers, which determine device performance [29]. ZnO belongs to the wurtzite space group C_{6v}^4 with two formula units in the primitive cell. The optical phonons at the Γ point of the Brillouin zone belong to the following irreducible representation [30]:

$$\Gamma_{opt} = 1A_1 + 2B_1 + 1E_1 + 2E_2 \quad (1)$$

where A_1, E_1 and $2E_2$ are Raman active modes, while $2B_1$ is the forbidden mode of ZnO [31]. The observed Raman spectrum of the ZnO lattice includes a transverse E_2 line at 437 cm^{-1}, a broad band from 540 cm^{-1} to 670 cm^{-1}, in which are the A_1(LO) line, the E_1(LO) line and other multi-phonon lines, between them being the two E_2 lines [30,31]. Fig. 6 shows the Raman measurements of the annealed Zn and Au pre-coated Zn foils. In the annealed Au pre-coated Zn foil, the Raman peaks at 273 cm^{-1} and 293 cm^{-1}, 420 cm^{-1} and the broad peak at 560 cm^{-1} which are referred to as the E_2(high)–E_2(low), E_2(high) and E_1(longitudinal-optic(LO)) modes, respectively. The E_2 (high)–E_2(low) (multi-phonon process i.e. 273 cm^{-1} and 293 cm^{-1}) mode can be found only when the ZnO is a single crystal. The E_2 (high) (i.e. 420 cm^{-1}) mode is a characteristic peak of wurtzite hexagonal ZnO, confirming that the grown nanowires are of

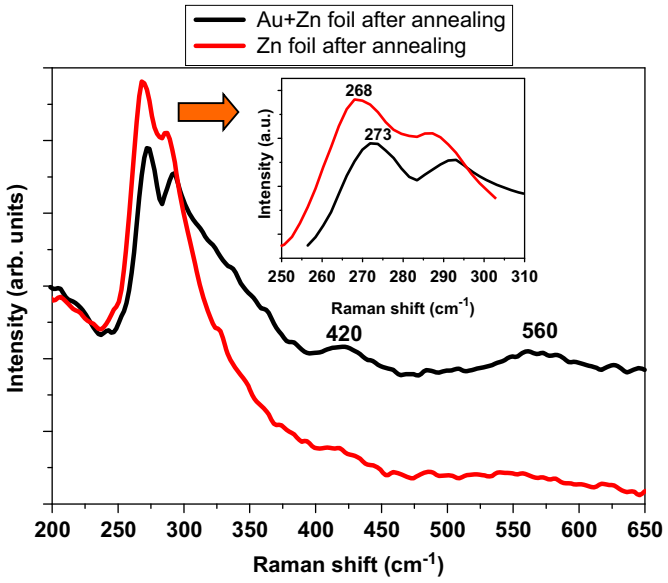

Fig. 6. Raman spectra of the Zn and Au pre-coated Zn foils annealed at 400 °C for 4 h. The inset shows the enlarged peaks in the range 250–310 cm^{-1}. The peak shift is around 5 cm^{-1}.

wurtzite hexagonal phase. No E_2(high) peak was detected for the annealed Zn foil, while the annealed Au pre-coated Zn foil shows a peak for E_2(high). Therefore, use of Au as a catalyst could improve the crystalline quality of the film. This result is in good agreement with the XRD and PL results. The E_1(LO) (i.e. 560 cm^{-1}) mode is associated with impurities and formation of defects such as oxygen vacancies, zinc interstitials, impurities, etc. [32]. In addition, the inset shows that Raman peaks of the annealed Au pre-coated Zn foil are blueshifted in comparison to those of the annealed Zn foil. It is known that blueshift of the Raman peaks indicate a decrease in oxygen vacancies [33]. This result is consistent with the PL data.

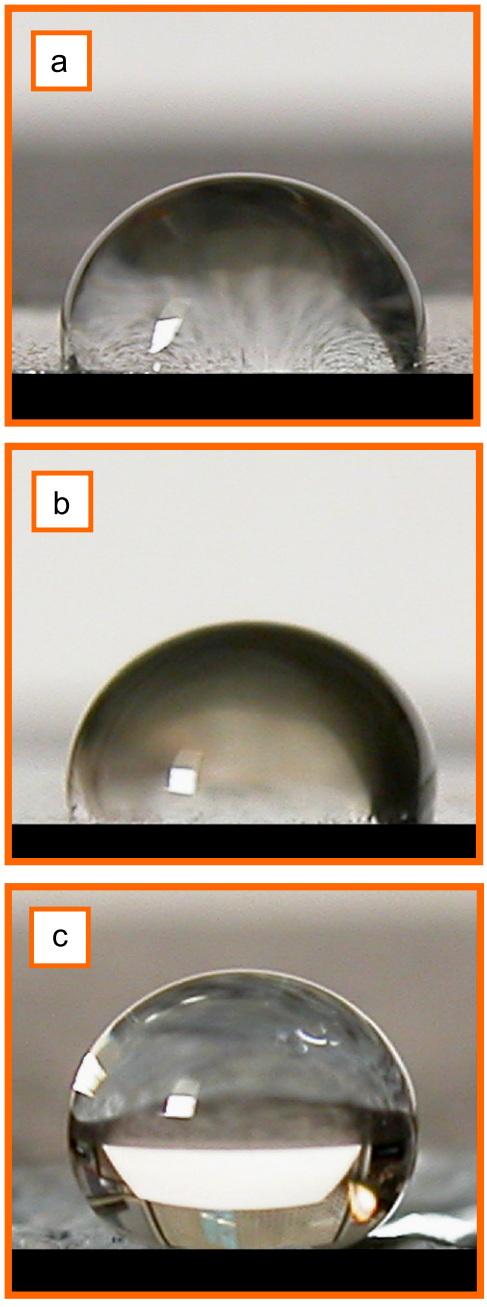

Fig. 7. Water contact angle images of the Zn foil (a), Au pre-coated Zn foil before (b) and after (c) annealing at 400 °C for 4 h.

Controlling and modifying the surface wettability are important in many practical applications [34]. Surface morphology and surface energy are two crucial factors to control the surface wettability. Thus, by changing the roughness of the surface and/or coating with other materials, the wetting characteristics are expected to be modified. In general, the surface wettability is determined by its WCA and divided into two categories, hydrophilic (WCA < 90°) and hydrophobic (WCA > 90°). Fig. 7 shows the WCA measurement of Zn foil, and the pre and post-annealed Au pre-coated Zn foil. It is observed that the WCAs of the specimens (Fig. 7(a)–(c)) are 91°, 95° and 155°, correspondingly. Thus, after annealing, the WCA has been observed to increase to 155°, which indicates a change in surface properties from hydrophilic to highly hydrophobic (WCA > 150°). This is consistent with the fact that hydrophobicity of surfaces improves when there is more air trapped between water and the rough surface. The changing wettability of ZnO nanowire film from hydrophilic to highly hydrophilic by an annealing process has also been studied by Meng et al. [35]. They found that the variation originates from excess oxygen ions on the wire surface. Shan et al. suggested that wettability could be influenced by O–H groups on the surface [36]. The XPS spectrum of O 1s (Fig. 4(c)) shows the presence of absorbed oxygen and O–H groups on the surface of the annealed specimen. The change could be attributed to the increase in roughness which leads to air being trapped on the surface. From this we conclude that the presence of absorbed oxygen and O–H groups on the surface combined with the increase in roughness caused an increase in the WCA between the solid and water [37].

4. Conclusions

Au–ZnO nanowire films have been prepared by annealing Zn foil pre-coated with a thin layer of gold. XRD studies revealed that the annealed film is polycrystalline in nature, possessing the wurtzite hexagonal phase. SEM images showed the presence of wire morphology on the entire surface of annealed Au–ZnO film. Gaussian fitting the results of the XPS spectrum of Au 4f–Zn 3p indicated that Au atoms are in an oxidation state. The XPS spectrum of Zn 2p showed that the split value of binding energy could be a characteristic value of ZnO. Two distinct components of O 1s were fitted by Gaussian deconvolution, which indicates oxygen deficiency on the film. The PL results show that as a result of the annealing process, the overall intensity of spectra is reduced due to a decrease in the concentration of oxygen vacancies on the surface of the ZnO. In addition, Raman measurements show that the crystalline quality of the films improved. All these could also provide evidence for the highly hydrophobic nature of Au–ZnO nanowire films.

Acknowledgments

This work was financially supported by the Islamic Azad University, Ahwaz Branch, Ahwaz, Iran. F. Jamali-Sheini

is grateful to Prof. P.B. Vidyasagar (Head of Department), Prof. D.S. Joag, and Dr. M.A. More from the Department of Physics, University of Pune, India, for their instrumentation support. R. Yousefi gratefully acknowledges the Islamic Azad University, Masjed-Soleiman Branch, for financial support in this research work.

References

[1] Ü. Özgür, Ya.I. Alivov, C. Liu, A. Teke, M.A. Reshchikov, S. Doğan, V. Avrutin, S.J. Cho, H. Morkoç, A comprehensive review of ZnO materials and devices, Applied Physics 98 (2005) 041301–041404.

[2] L.E. Halliburton, N.C. Giles, N.Y. Garces, M. Luo, C. Xu, L. Bai, L.A. Boatner, Production of native donors in ZnO by annealing at high temperature in Zn vapor, Applied Physics Letters 87 (2005) 172108–172110.

[3] B. Xiang, P. Wang, X. Zhang, S.A. Dayeh, D.P.R. Aplin, C. Soci, D. Yu, D. Wang, Rational synthesis of p-type zinc oxide nanowire arrays using simple chemical vapor deposition, Nano Letters 7 (2007) 323–328.

[4] F. Jamali-Sheini, K.R. Patil, D.S. Joag, M.A. More, Synthesis of Cu–ZnO and C–ZnO nanoneedle arrays on zinc foil by low temperature oxidation route: effect of buffer layers on growth, optical and field emission properties, Applied Surface Science 257 (2011) 8366–8372.

[5] J. Xiao, X. Zhang, G. Zhang, Field emission from zinc oxide nanotowers: the role of the top morphology, Nanotechnology 19 (2008) 295706–295712.

[6] R. Yousefi, M.R. Muhamad, A.K. Zak, The effect of source temperature on morphological and optical properties of ZnO nanowires grown using a modified thermal evaporation set-up, Current Applied Physics 11 (2011) 767–770.

[7] Y. Wu, Z. Xi, G. Zhang, J. Zhang, D. Guo, Fabrication of hierarchical zinc oxide nanostructures through multistage gas-phase reaction, Crystal Growth and Design 8 (2008) 2646–2651.

[8] Y. Zhang, R.E. Russo, S.S. Mao, Femtosecond laser assisted growth of ZnO nanowires, Applied Physics Letters 87 (2005) 133115–133118.

[9] R.F. Zhuo, H.T. Feng, J.T. Chen, D. Yan, J.J. Feng, H.J. Li, B.S. Geng, S. Cheng, X.Y. Xu, P.X. Yan, Multistep synthesis, growth mechanism, optical, and microwave absorption properties of ZnO dendritic nanostructures, Journal of Physical Chemistry C 112 (2008) 11767–11775.

[10] C.X. Shan, Z. Liu, Z.Z. Zhang, D.Z. Shen, S.K. Hark, A simple route to porous ZnO and ZnCdO nanowires, The Journal of Physical Chemistry B 110 (2006) 11176–11179.

[11] Y. Chen, H.J. Ko, S.K. Hong, T. Yao, Layer-by-layer growth of ZnO epilayer on Al_2O_3(0001) by using a MgO buffer layer, Applied Physics Letters 76 (2000) 559–561.

[12] S.K. Na Ayudhya, P. Tonto, O. Mekasuwandumrong, V. Pavarajarn, P. Praserthdam, Solvothermal synthesis of ZnO with various aspect ratios using organic solvents, Crystal Growth and Design 6 (2006) 2446–2450.

[13] S.H. Jung, E. Oh, K.H. Lee, Y. Yang, C.G. Park, W. Park, S.-H. Jeong, Sonochemical preparation of shape-selective ZnO nanostructures, Crystal Growth and Design 8 (2008) 265–269.

[14] S. Peulon, D. Lincot, Cathodic electrodeposition from aqueous solution of dense or open-structured zinc oxide films, Advanced Materials 8 (1996) 166–170.

[15] F. Jamali Sheini, I.S. Mulla, D.S. Joag, M.A. More, Influence of process variables on growth of ZnO nanowires by cathodic electrodeposition on zinc substrate, Thin Solid Films 517 (2009) 6605–6611.

[16] N. Hongsith, C. Viriyaworasakul, P. Mangkorntong, N. Mangkorntong, S. Choopun, Ethanol sensor based on ZnO and Au-doped ZnO nanowires, Ceramics International 34 (2008) 823–826.

[17] N.S. Ramgir, Y.K. Hwang, S.H. Jhung, H.K. Kim, J.S. Hwang, I.S. Mulla, J.S. Chang, CO sensor derived from mesostructured Au-doped SnO_2 thin film, Applied Surface Science 252 (2006) 4298–4305.

[18] X. Wang, J. Zhang, Z. Zhu, J. Zhu, Humidity sensing properties of Pd^{2+}-doped ZnO nanotetrapods, Applied Surface Science 253 (2007) 3168–3173.

[19] G. Neri, A. Bonavita, G. Micali, G. Rizzo, N. Pinna, M. Niedeberger, In_2O_3 and Pt–In_2O_3 nanopowders for low temperature oxygen sensors, Sensors and Actuators B 127 (2007) 455–462.

[20] C. Yang, U. Tartaglino, B.N.J. Persson, Influence of surface roughness on super hydrophobicity, Physical Review Letters 97 (2006) 116103–116106.

[21] R. Paul, S.N. Das, S. Dalui, R.N. Gayen, R.K. Roy, R. Bhar, A.K. Pal, Synthesis of DLC films with different sp2/sp3 ratios and their hydrophobic behaviour, Journal of Physics D: Applied Physics 41 (2008) 055309.

[22] G.E. Muilenbenger (Ed.), Handbook of X-ray Photoelectron Spectroscopy, Perkin-Elmer Corporation, Minnesota, 1979.

[23] A.B. Djurisic, Y.H. Leung, K.H. Tam, Y.F. Hsu, L. Ding, W.K. Ge, Y.C. Zhong, K.S. Wong, W.K. Chan, H.L. Tam, K.W. Cheah, W.M. Kwok, D.L. Phillips, Defect emissions in ZnO nanostructures, Nanotechnology 18 (2007) 095702–095709.

[24] S. Fujihara, Y. Ogawa, A. Kasai, Tunable visible photoluminescence from ZnO thin films through Mg-doping and annealing, Chemistry of Materials 16 (2004) 2965–2968.

[25] K. Vanheusden, C.H. Seager, W.L. Warren, D.R. Tallant, J.A. Voigt, Correlation between photoluminescence and oxygen vacancies in ZnO phosphors, Applied Physics Letters 68 (1996) 403–405.

[26] K. Vanheusden, W.L. Warren, C.H. Seager, D.R. Tallant, J.A. Voigt, B.E. Gnade, Mechanisms behind green photoluminescence in ZnO phosphor powders, Journal of Applied Physics 79 (1996) 7983–7990.

[27] F. Jamali Sheini, D.S. Joag, M.A. More, J. Singh, O.N. Srivasatva, Low temperature growth of aligned ZnO nanowires and their application as field emission cathodes, Materials Chemistry and Physics 120 (2010) 691–696.

[28] R. Yousefi, B. Kamaluddin, Effect of S- and Sn-doping to the optical properties of ZnO nanobelts, Applied Surface Science 255 (2009) 9376–9380.

[29] C. Bundesmann, N. Ashkenov, M. Schubert, D. Spemann, T. Butz, E.M. Kaidashev, M. Lorenz, M. Grundmann, Raman scattering in ZnO thin films doped with Fe, Sb, Al, Ga and Li, Applied Physics Letters 83 (2003) 1974–1976.

[30] T.C. Damen, S.P.S. Porto, B. Tell, Raman effect in zinc oxide, Physical Review 142 (1966) 570–574.

[31] J.M. Calleja, M. Cardona, Physical Review B 16 (1977) 3753–3761.

[32] Y.J. Xing, Z.H. Xi, Z.Q. Xue, X.D. Zhang, J.H. Song, R.M. Wang, J. Xu, Y. Song, S.L. Zhang, D.P. Yu, Optical properties of the ZnO nanotubes synthesized via vapor phase growth, Applied Physics Letters 83 (2003) 1689–1691.

[33] F. Xiu, Z. Yang, D. Zhao, J. Liu, K.A. Alim, A.A. Balandin, M.E. Itkis, R.C. Haddon, ZnO growth on Si with low-temperature ZnO buffer layers by ECR-assisted MBE, Journal of Crystal Growth 286 (2006) 61–65.

[34] I.P. Parkin, G.R. Palgrave, Self-cleaning coatings, Journal of Materials Chemistry 15 (2005) 1689–1695.

[35] X.Q. Meng, D.X. Zhao, J.Y. Zhang, D.Z. Shen, Y.M. Lu, L. Dong, Z.Y. Xiao, Y.C. Liu, X.W. Fan, Wettability conversion on ZnO nanowire arrays surface modified by oxygen plasma treatment and annealing, Chemical Physics Letters 413 (2005) 450–453.

[36] M.H. Shang, Y. Wang, K. Takahashi, G.Z. Cao, D. Li, Y.N. Xia, Nanostructured superhydrophobic surfaces, Journal of Materials Science 40 (2005) 3587–3591.

[37] C.Y. Kuan, M.H. Hon, J.M. Chou, I.C. Leu, Wetting characteristics on micro/nanostructured zinc oxide coatings, Journal of the Electrochemical Society 156 (2) (2009) J32–J36.